

A 3D model for earthquake-induced liquefaction triggering and post-liquefaction response



Arash Khosravifar^{a,*}, Ahmed Elgamal^b, Jinchi Lu^b, John Li^b

^a Department of Civil and Environmental Engineering, Portland State University, Portland, OR 97201, USA

^b Department of Structural Engineering, University of California, San Diego, La Jolla, CA 92093, USA

ARTICLE INFO

Keywords:

Liquefaction
Constitutive modeling
Plasticity
Triggering
Cyclic mobility

ABSTRACT

A constitutive soil model that was originally developed to model liquefaction and cyclic mobility has been updated to comply with the established guidelines on the dependence of liquefaction triggering to the number of loading cycles, effective overburden stress ($K\sigma$), and static shear stress ($K\alpha$). The model has been improved with new flow rules to better capture contraction and dilation in sands and has been implemented as PDMY03 in different computational platforms such as OpenSees finite-element, and FLAC and FLAC^{3D} finite-difference frameworks. This paper presents the new modified framework of analysis and describes a guideline to calibrate the input parameters of the updated model to capture liquefaction triggering and post-liquefaction cyclic mobility and the accumulation of plastic shear strain. Different sets of model input parameters are provided for sands with different relative densities. Model responses are examined under different loading conditions for a single element.

1. Introduction

Soil liquefaction has been shown to be a major cause of damage to structures in past earthquakes. Several constitutive models have been developed to capture various aspects of flow liquefaction and cyclic mobility such as Manzari and Dafalias [21], Cubrinovski and Ishihara [8], Li and Dafalias [20], Byrne and McIntyre [6], and Papadimitriou et al. [25] to name a few. Simulating soil liquefaction using numerical models offers several challenges including: (a) reasonably capturing triggering of liquefaction or the rate of pore-water-pressure (PWP) generation for sands with different relative densities under various levels of shear stress, effective overburden stress and static shear stress, and (b) post-liquefaction cycle-by-cycle accumulation of shear and volumetric strains.

A constitutive model was developed within classical multi-surface plasticity formulation by using a mixed stress- and strain- space yield domain to reasonably capture soil liquefaction and specifically replicate the large shear strains that occur at minimal change in stress state in laboratory results [26,33]. This model was implemented into a solid-fluid fully-coupled OpenSees finite element (FE) framework ([26,7] and [23]). The first version of the multi-yield surface pressure dependent model (PDMY) was developed primarily to capture post-liquefaction cyclic softening mechanism and the accumulation of plastic shear deformations. The previous calibration was performed against a dataset of

laboratory and centrifuge tests and the model parameters were provided for sands with different relative densities in Yang et al. [32] and Elgamal et al. [10]. The original experimental dataset was rather limited in terms of pore-water-pressure build up; therefore, liquefaction triggering was not the primary focus in the development of the original constitutive model and the calibration was performed including engineering judgment. Since new data and established procedures that have been under development in the past 30–40 years have become available, it became possible to make updates to the constitutive model to capture factors that affect triggering of liquefaction, as will be explained in the following paragraphs.

Various studies employing different analytical or experimental methods have been performed in recent years that provide insights on factors that affect triggering of liquefaction. Laboratory tests have shown the effect of number of loading cycles on the cyclic shear strength of sands (e.g. [34]). Laboratory tests, case histories and theoretical studies using critical-state soil mechanics suggest that the cyclic shear strength of sands against the triggering of liquefaction is affected by the effective overburden stress characterized by the $K\sigma$ factor (e.g. [4]). Furthermore, laboratory tests have shown that the cyclic resistance of sands against the triggering of liquefaction is affected by initial static shear stress which is often characterized by the $K\alpha$ factor [12,5]. To be able to capture these effects in the model response, the contraction and dilation equations in the constitutive model were

* Corresponding author.

E-mail address: karash@pdx.edu (A. Khosravifar).

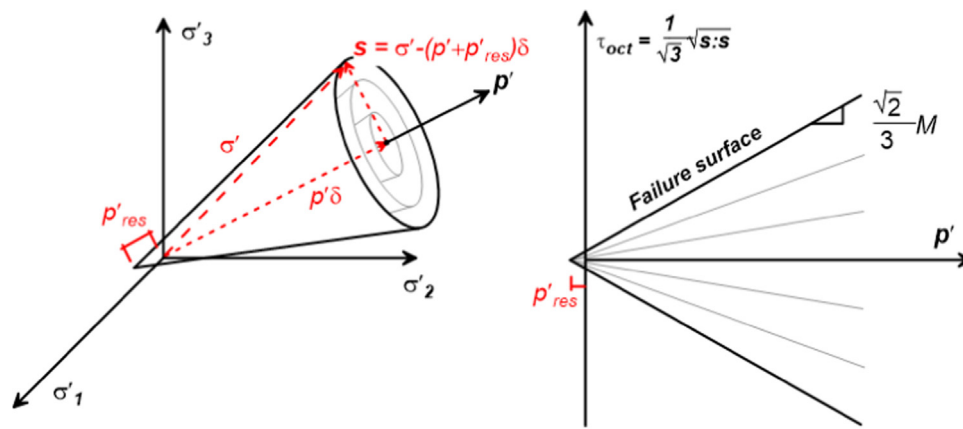


Fig. 1. Conical multi-surface yield criteria in principal stress space.

updated with a new set of equations. Specific attention was given to capture the dependency of liquefaction triggering on the number of loading cycles, effective overburden stress, and initial static shear stress. We took a model that had certain strengths in capturing post-liquefaction cyclic softening and strain accumulation, and updated it into a practical tool that can reliably capture the rate of pore-water-pressure generation, triggering of liquefaction at different number of loading cycles, overburden stress ($K\sigma$) and static shear stress ($K\alpha$) in both 2D and 3D applications.

This paper presents the basic formulation of the new model and provides calibrated parameters for sands with different relative densities. The focus of this paper is to show how the new model can capture the effects of various factors discussed above on liquefaction triggering. Despite the many input parameters required by the model, the calibration is developed with a goal to derive model input parameters using minimal data available to user (i.e. the relative density) and filling the gaps using design correlations. The calibration process has been primarily based on the correlations proposed by Idriss and Boulanger [14] for liquefaction triggering curves. A similar calibration process can be followed when lab data are available or if other triggering correlations are chosen. The model responses are illustrated for single-element simulations under undrained-cyclic loading conditions.

The updated model has been implemented in OpenSees finite-element, and FLAC and FLAC^{3D} finite-difference frameworks as PDMY03. The results shown in this paper are created using OpenSees framework; however, similar results can be obtained using FLAC or FLAC^{3D}. The source code for this model is available in public domain as part of the OpenSees computational framework (<http://opensees.berkeley.edu>). A user manual, a library of example files, element drivers and post-processors are available and maintained at <http://soilquake.net/>.

In FLAC, the solid domain is discretized by a finite difference mesh consisting of quadrilateral elements or zones [15]. Each element is subdivided internally by its diagonals into two overlaid sets of constant-strain triangular sub-elements or subzones (resulting in four sub-elements in total for each quadrilateral element). FLAC employs a “mixed discretization technique” [22] to overcome the mesh-locking problem: The isotropic stress and strain components are taken to be constant over the whole quadrilateral element, while the deviatoric components are maintained separately for each triangular sub-element [15]. Similarly, the above-mentioned mixed discretization approach is also applied in FLAC^{3D} [16] where each 8-node hexahedral element or zone is subdivided into 10 tetrahedral sub-elements.

In the soil model implementation, each sub-element (analogous to a Gauss integration point in Finite Element method) is treated independently. A complete set of soil modeling parameters including stress state and yield surface data is maintained separately for each sub-element. At each time step, the soil model is called to obtain a new stress state for each sub-element given the strain increments of the sub-

elements.

For FLAC and FLAC3D, site response simulations (shear beam-type response) have shown that the stress state of subzones of any given element were virtually identical and similar to the overall averaged FLAC/FLAC3D response for the element. However, further work might be required to enforce additional constraints on the sub-zone responses for general scenarios of 2D/3D soil and soil-structure interaction responses as highlighted in the works of Andrianopoulos et al. [1], Zi-topoulou and Boulanger [35], and Beaty [3]. This effort is currently underway.

Originally, the soil modeling code was implemented in OpenSees (written in Visual C++). The implementation in FLAC and FLAC^{3D} mainly involved the addition of interfaces between FLAC (or FLAC^{3D}) and the existing OpenSees soil model code. It was verified that similar results are obtained using FLAC, FLAC^{3D} and OpenSees for the implemented model. As such, the soil constitutive model has been compiled as a dynamic link library (DLL) with corresponding versions for FLAC (Versions 7 and 8) and FLAC^{3D} (Versions 5 and 6).

2. Constitutive model formulation

Based on the original multi-surface plasticity framework of Prevost [27], the model incorporates a non-associative flow rule and a strain-space mechanism [10,32] in order to reasonably simulate cyclic mobility response features. This section will briefly define the components of the material plasticity including yield function, hardening rule and flow rule. Further details on model formulations are provided in Yang and Elgamal [33] and Yang et al. [32].

2.1. Yield surface

The yield function in this model is defined as conical shape multi-surfaces with a common apex located at the origin of the principal space (Fig. 1). The outermost surface defines the yield criterion and the inner surfaces define the hardening zone [17,24,27]. It is assumed that the material elasticity is linear and isotropic, and that nonlinearity and anisotropy results from plasticity [13].

The model is implemented in the octahedral space and it is important to differentiate the horizontal plane shear stress (and strain) in 2D modeling from octahedral shear stress (and strain) in 2D and 3D modeling. The deviatoric stress is defined in Fig. 1 as $\tilde{\sigma} = \sigma' - p'\mathbf{I}$ and the second invariant of deviatoric stress tensor is defined as $J_2 = \frac{1}{2}[\tilde{\sigma} : \tilde{\sigma}]$. The octahedral shear stress (τ_{oct}) is defined as:

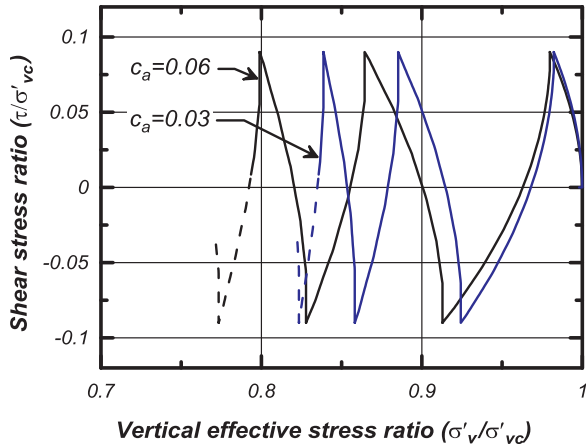


Fig. 2. Effects of input parameter c_a on contraction rate.

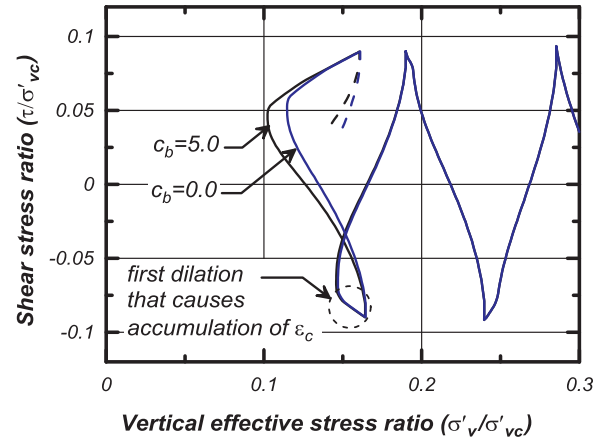


Fig. 3. Effects of input parameter c_b (fabric damage) on contraction rate.

$$\begin{aligned} \tau_{\text{oct}} &= \frac{1}{\sqrt{3}} \sqrt{\tilde{\mathbf{s}} : \tilde{\mathbf{s}}} \\ &= \frac{1}{3} \sqrt{(\sigma'_{11} - \sigma'_{22})^2 + (\sigma'_{22} - \sigma'_{33})^2 + (\sigma'_{11} - \sigma'_{33})^2 + 6\sigma'_{12}{}^2 + 6\sigma'_{13}{}^2 + 6\sigma'_{23}{}^2} \end{aligned} \quad (1)$$

The yield surfaces are defined by setting the second invariant of the deviatoric stress tensor to a constant. In this case the constant is $M^2 p'^2/3$ where M defines the size of the yield surfaces and is related to the soil friction angle for the outermost yield surface. Consequently, the conical yield surface equations are defined as:

$$3J_2 = M^2 (p' + p'_{\text{res}})^2 \quad (2)$$

where, p'_{res} is a small positive constant that defines shear strength at zero effective confining stress. This variable will not be repeated in following equations for simplicity. Combining Eqs. 1 and 2 we get the following general relationship:

$$M = \frac{3}{\sqrt{2}} \frac{\tau_{\text{oct}}}{p'} \quad (3)$$

The parameter M (in the yield surface equation) can be selected to match the shear strength exhibited in a particular stress path. The 3D implementation of the equations requires that the user modifies the input friction angle in order to define any desired level of shear strength within the range defined by Triaxial compression/extension and/or simple shear.

2.2. Modulus reduction curves (G/G_{max})

The strain vector is divided into deviatoric and volumetric components. The deviatoric strain is defined in octahedral space as:

$$\gamma_{\text{oct}} = \frac{2}{3} \sqrt{(\epsilon_{11} - \epsilon_{22})^2 + (\epsilon_{22} - \epsilon_{33})^2 + (\epsilon_{11} - \epsilon_{33})^2 + 6\epsilon_{12}{}^2 + 6\epsilon_{13}{}^2 + 6\epsilon_{23}{}^2} \quad (4)$$

Note that $\epsilon_{12} = \frac{1}{2}\gamma_{12}$, where γ_{12} is the horizontal shear strain commonly used in engineering practice. The relationship between τ_{oct} and γ_{oct} is defined using the shear modulus. The shear modulus at small-strains (G_{max}) is stress-dependent as defined in the equation below:

$$G_{\text{max}} = G_{\text{max,r}} \left(\frac{p'}{p'_r} \right)^d \quad (5)$$

where, $G_{\text{max,r}}$ is the small-strain shear modulus at the reference effective confining stress (p'_r) specified by the user, d is the stress-dependency input parameter which is typically selected as 0.5 for sands [18], and p' is the effective confining stress that usually changes during undrained loading.

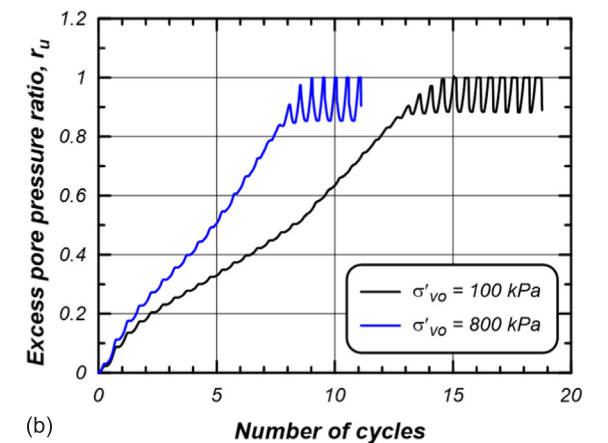
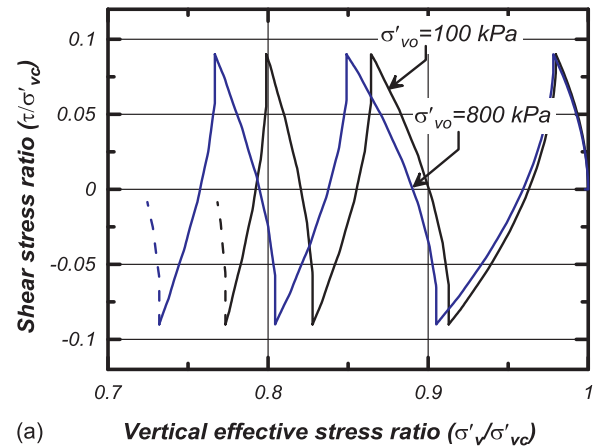


Fig. 4. Effects of overburden stress on contraction rate (K_σ effect) for input parameter $c_c = 0.2$; (a) stress path and (b) pore water pressure ratio versus number of shear cycles.

The shear modulus reduction curves (G/G_{max} curve) are defined either by the code-generated hyperbolic (backbone) curve, or by a user-defined modulus-reduction curve. The code-generated hyperbolic curve is adequate for modeling liquefaction where the soil responses in undrained-cyclic conditions. For modeling the drained-cyclic behavior (such as total-stress site-response analysis) the user-defined modulus-reduction curves may be more suitable to obtain the desired hysteretic loops. The shape of the code-generated hyperbolic curve is stress-dependent as defined in the equation below:

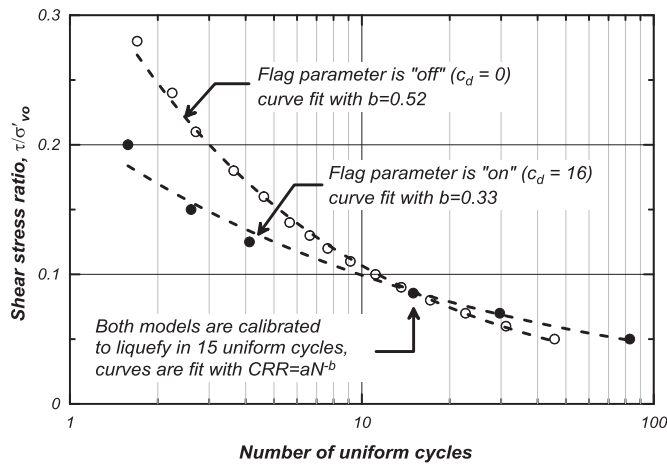


Fig. 5. Effects of input parameter c_d on the number of uniform loading cycles to trigger liquefaction.

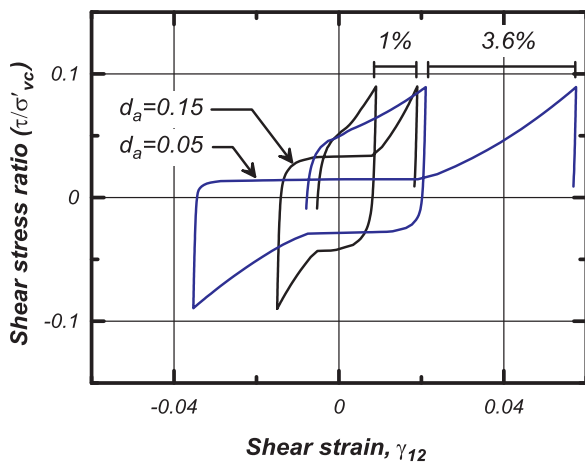


Fig. 6. Effects of input parameter d_a on dilation rate.

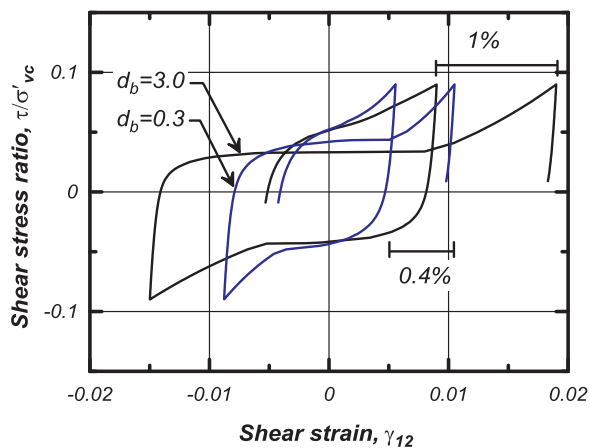


Fig. 7. Effects of input parameter d_b (fabric damage) on dilation rate.

$$\tau_{oct} = \frac{G_{max}}{1 + \frac{\gamma_{oct}}{\gamma_r} \left(\frac{p'_r}{p'}\right)^d} (\gamma_{oct}) \quad (6)$$

where, G_{max} is the small-strain shear modulus at an effective confining stress p' , and p'_r is the reference effective confining stress defined previously. Parameter d is a model input parameter that defines the change in the shape of the backbone curve with respect to the effective confining stress (this is the same parameter defined above that defines the

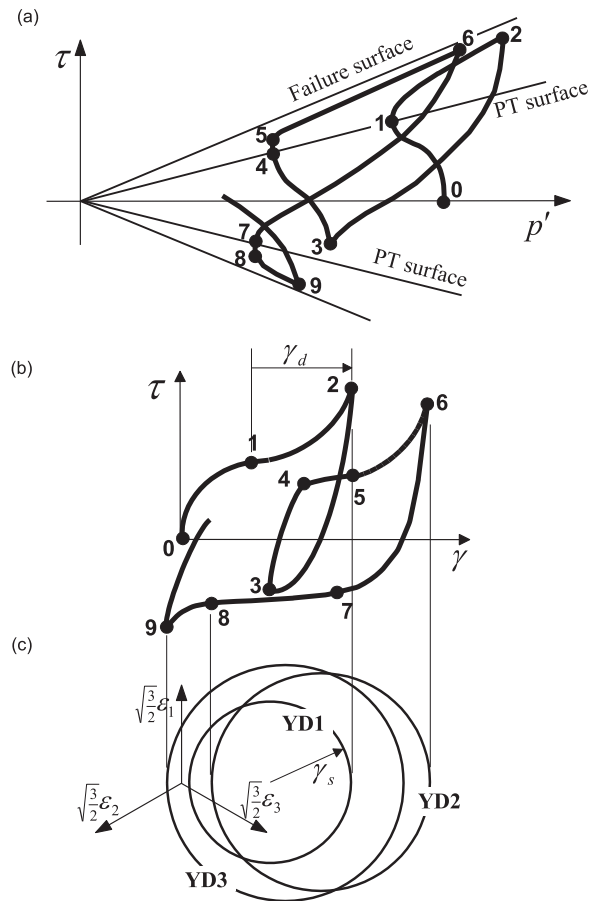


Fig. 8. Schematic of the neutral phase in model response showing (a) octahedral stress τ - effective confinement p' response, (b) τ - octahedral strain γ response, and (c) configuration of yield domain.

dependency of G_{max} to the effective confining stress). γ_r is an internally-calculated shear strain to define the shape of the backbone curve.

Alternatively, the model provides the flexibility to manually define the shear stress-strain relationship by specifying the modulus reduction curve in a form of pairs of G/G_{max} and γ_{12} . Methods to define strength compatible modulus reduction curves are described in detail in Gingery and Elgamal [11].

2.3. Hardening rule

Following Mroz [24] and Prevost [27], a purely deviatoric kinematic hardening rule was employed to generate hysteretic response. This rule maintains the Mroz [24] concept of conjugate-points contact, with slight modifications in order to enhance computational efficiency [10,26]. For drained cyclic shear loading, this means that the model essentially exhibits Masing loading/unloading behavior.

2.4. Flow rule

The flow rule equations (contraction and dilation) in the original model were developed primarily to capture the cyclic mobility mechanism including the accumulation of post-liquefaction plastic shear strains and the subsequent dilative phases observed in liquefied soil response. The new updates to the flow rules enable the user to better control the rate of pore-water-pressure generation and subsequently the triggering of liquefaction.

Plastic strain increments are defined using outer normal tensors to the yield surface (\hat{Q}) and to the plastic potential surface (\hat{P}). These normal tensors are decomposed into deviatoric and volumetric

Table 1
Model input parameters.

Model parameters	Loose sand	Medium dense sand	Dense sand	Very dense sand
$(N_1)_{60}^a$	5	15	25	35
Relative density, D_R^a	33%	57%	74%	87%
Cyclic resistance ratio, $CRR_{\sigma'_v=1, M=7.5}^a$	0.09	0.16	0.29	N.A.
Density, ρ	1.94 t/m ³	1.99 t/m ³	2.03 t/m ³	2.06 t/m ³
Reference mean effective pressure, p'_r	101 kPa	101 kPa	101 kPa	101 kPa
Small-strain shear modulus at reference pressure, $G_{max,r}$	46.9 MPa	73.7 MPa	94.6 MPa	111.9 MPa
Maximum shear strain at reference pressure, $\gamma_{max,r}$	0.1	0.1	0.1	0.1
Bulk modulus at reference pressure, B_r	125.1 MPa	196.8 MPa	252.6 MPa	298.3 MPa
Pressure dependence coefficient, d	0.5	0.5	0.5	0.5
DSS friction angle, ϕ_{DSS}^a	30°	35°	40°	45°
Model friction angle, ϕ	25.4°	30.3°	35.8°	42.2°
Phase transformation angle, ϕ_{PT}	20.4°	25.3°	30.8°	37.2°
Contraction coefficient, c_a	0.03	0.012	0.005	0.001
Contraction coefficient, c_b	5.0	3.0	1.0	0.0
Contraction coefficient, c_c	0.2	0.4	0.6	0.8
Contraction coefficient, c_d	16.0	9.0	4.6	2.2
Contraction coefficient, c_e	2.0	0.0	-1.0	0.0
Dilation coefficient, d_a	0.15	0.3	0.45	0.6
Dilation coefficient, d_b	3.0	3.0	3.0	3.0
Dilation coefficient, d_c	-0.2	-0.3	-0.4	-0.5
Number of yield surfaces, NYS	20	20	20	20
S_0	1.73 kPa	1.73 kPa	1.73 kPa	1.73 kPa

^a These are not input parameters to the constitutive model, but rather parameters computed during model calibration.

components, giving $\tilde{Q} = \tilde{Q}' + Q''\tilde{I}$ and $\tilde{P} = \tilde{P}' + P''\tilde{I}$, where \tilde{Q}' and \tilde{P}' are the deviatoric components, and $Q''\tilde{I}$ and $P''\tilde{I}$ are the volumetric components [27]. In this model, the deviatoric component of the plastic strain increment follows an associative flow rule ($\tilde{P}' = \tilde{Q}'$); while, the volumetric component of the plastic strain increment follows non-associative flow rule ($P'' \neq Q''$).

Consequently, P'' is defined distinctively based on the relative location of the stress state with respect to the Phase Transformation (PT) surface, η , defined as $\eta = \sqrt{3}(\tilde{s} : \tilde{s})/2/p'$. Similarly, η_{PT} is defined as the stress ratio along the PT surface. It follows that the value of η and the sign of $\dot{\eta}$ (the time rate of η) determine distinct contractive and dilative behavior of material under shear loading, as described in the next two sections.

2.4.1. Contractive phase

Shear-induced contraction occurs inside the PT surface ($\eta < \eta_{PT}$), as well as outside ($\eta > \eta_{PT}$) when $\dot{\eta} < 0$. The adopted sign convention is such that normal stresses are positive in compression. The contraction flow rule is defined as:

$$P'' = -C \left(1 - \text{sign}(\dot{\eta}) \frac{\eta}{\eta_{PT}} \right)^2 (c_a + \epsilon_c c_b) \left(\frac{p'}{p_{atm}} \right)^{c_c} \quad (7a)$$

$$C = [1 + (c_d \cdot |CSR - CSR_0|)^3] \times [1 + c_e \cdot CSR_0]^2 \quad (7b)$$

$$CSR = \frac{\sqrt{\tau_1^2 + \tau_2^2 + \tau_3^2}}{p'_0} \quad (7c)$$

where, c_a to c_e are model input parameters. ϵ_c is a non-negative scalar that represents the accumulative volumetric strain (it increases by dilation and decreases by contraction). The term $\epsilon_c c_b$ is a means to account for the fabric damage in a simplified approach, i.e. a strong dilation results in higher contraction in the subsequent unloading cycle. This behavior is observed in experiments and is accounted for in various degrees of robustness in other similar constitutive models [25,9]. The C parameter encapsulates new updates to capture the effects of the number of loading cycles and the static shear stress, which will be described later in this section. The c_a and c_b parameters were in the original model. To preserve the continuity with the original model we kept the shape of the equation.

The effect of input parameter c_a on the contraction rate is shown in Fig. 2 for an undrained cyclic simple shear simulation on a single

element. Stronger contraction results in faster pore water pressure build-up and larger reduction in the vertical effective stress.

The effect of input parameter c_b on the contraction rate is shown in Fig. 3 for an undrained cyclic simple shear simulation. The first dilation is denoted in the figure. In the case where fabric damage is activated (i.e. $c_b = 5.0$) the accumulated volumetric strain (ϵ_c) in the first dilation results in a more contractive behavior in the subsequent unloading cycle.

One of the main improvements to the original model was made by incorporating the effects of effective overburden stress on the contraction rate, also known as the k_σ effect. This effect is controlled through an input parameter c_c and is shown in Fig. 4. A sample with higher initial effective overburden stress ($\sigma'_{vo} = 800kPa$) tends to be more contractive compared to a sample with smaller initial effective overburden stress ($\sigma'_{vo} = 100kPa$) when subjected to the same shear stress ratio (τ_2/σ'_{vo}) in an undrained simple shear simulation.

Additional improvements to the constitutive model were made by introducing parameter C to the contraction equation as shown in Eqs. 7b and 7c. The variables CSR and CSR_0 are the shear stress ratios, and P'_0 is the initial mean effective stress. The index “0” in these variables denotes the initial value of the variables before the application of cyclic shear stress (after consolidation).

It is common to calibrate input parameters of the model to liquefy at a shear stress ratio corresponding to earthquake magnitude $M = 7.5$ and effective overburden stress $\sigma'_v = 1 \text{ atm}$ ($CSR_{M=7.5, \sigma'_v=1 \text{ atm}}$). This will anchor the CSR versus number of loading cycles curve to the point corresponding to the desired CSR and 15 uniform cycles (as shown for the two curves in Fig. 5). The experimental data show that the b -value of the power fit for curves in Fig. 5 should be approximately 0.34 for undisturbed frozen samples of clean sands [14,34]. The original model was found to have a b -value close to 0.52 (the curve with the flag parameter set to “off” or $c_d = 0$ in Fig. 5). The model response was improved in the updated model by introducing the first term on Eq. 7b (controlled by input parameter c_d). The updated model response has a b -value close to 0.33 (the curve with the flag parameter set to “on” or $c_d = 16$ in Fig. 5). It needs to be mentioned that other experimental studies on reconstituted sand samples suggest that the b -values can be much smaller than 0.34 (e.g. [29,30]). Calibration for such a lower b -value can be performed with a possible change of the exponent “3” in Eq. 7b. In this regard, additional work is currently underway.

The original model was also found to be relatively insensitive to the

Table 2
Description of calibration parameters.

Parameter	Description
$(N_1)_{60}$	Corrected SPT blow counts normalized for overburden stress of 1 atm.
D_R	Relative density correlated to SPT blow count using $D_R = \sqrt{\frac{(N_1)_{60}}{46}}$ from Idriss and Boulanger [14]
$CRR_{\sigma'_v=1, M=7.5}$	The cyclic stress ratio to trigger liquefaction under vertical effective stress of 1 atm in 15 uniform loading cycles (equivalent number of uniform cycles for a magnitude 7.5 earthquake based on [28]). Triggering of liquefaction is defined here as the moment at which the material reaches to a single-amplitude shear strain of 3%. Liquefaction triggering correlations by Idriss and Boulanger [14] were used in this calibration study: $CRR_{\sigma'_v=1, M=7.5} = \exp\left(\frac{(N_1)_{60}}{14.1} + \left(\frac{(N_1)_{60}}{126}\right)^2 - \left(\frac{(N_1)_{60}}{23.6}\right)^3 + \left(\frac{(N_1)_{60}}{25.4}\right)^4 - 2.8\right)$
p'_r	Reference mean effective pressure at which small-strain shear modulus ($G_{max,r}$) and bulk modulus (B_r) are specified. It is taken as 101 kPa (1 atm) in this calibration.
$G_{max,r}$	Small-strain shear modulus at the reference mean effective pressure (p'_r) of 1 atm. $G_{max,r}$ was calculated from the shear wave velocity estimates by Andrus and Stokoe [2] with slight modifications for very small blow counts by Ziotopoulou and Boulanger [35]: $V_{s,\sigma'_v=1} = 85[(N_1)_{60} + 2.5]^{0.25}$ where $V_{s,\sigma'_v=1}$ is the shear wave velocity at vertical effective stress of 1 atm. $G_{max,r}$ was adjusted by a factor of $\sqrt{3/2}$ to account for the change in confining pressure from $K_o = 0.5$ to 1.0 using $d = 0.5$ in Eq. (5).
$\gamma_{max,r}$	The octahedral shear strain at failure at the reference mean effective pressure p'_r . This parameter is set to 0.1 (10%) in this calibration.
B_r	The bulk modulus at reference pressure (p'_r) is derived from the small-strain shear modulus; $B_r = (B/G)G_{max,r}$. The bulk modulus to shear modulus ratio is derived from: $(B/G) = \frac{2(1+\nu)}{3(1-2\nu)} = 2.6$ using Poisson's ratio of $\nu = 0.33$
d	The pressure dependency coefficient defines the dependency of the small-strain shear modulus and the shape of the modulus reduction curves to the effective confining stress.
φ_{DSS}	Friction angle obtained from direct simple shear (DSS) test.
φ	The input friction angle that defines the size of the outermost yield surface. In order to achieve a desired shear strength obtained from DSS tests, the input friction angle can be calculated from the following equation: $\varphi = \sin^{-1}\left[\frac{3\tan(\varphi_{DSS})}{2\sqrt{3} + \tan(\varphi_{DSS})}\right]$
φ_{PT}	The phase transformation angle is the angle over which the soil behavior changes from contractive to dilative (usually a few degrees smaller than the soil friction angle).
c_a	This parameter is the main input parameter controlling the contraction rate and subsequently the pore-water-pressure generation rate (Eq. 7a). This parameter was calibrated to trigger liquefaction in 15 loading cycles at a cyclic stress ratio equal to $CRR_{\sigma'_v=1, M=7.5}$.
c_b	This parameter accounts for fabric damage. In the absence of reliable laboratory data that quantifies fabric damage, this parameter was calibrated in combination with other contraction parameters to capture the triggering of liquefaction.
c_c	This parameter accounts for the overburden stress effect (i.e. K_σ effect).
c_d	A new parameter introduced in the updated model to increase (decrease) the rate of contraction for large (small) shear stress ratios. This feature can be disabled by setting $c_d = 0$.
c_e	A new parameters introduced in the updated model to control the dependency of contraction rate to static shear stress ratio and achieve desired $K\alpha$. This feature can be disabled by setting $c_e = 0$.
d_a	This parameter, combined with the difference between φ and φ_{PT} , are the primary parameters to control the dilation tendency after crossing the PT surface. d_a was calibrated to produce the desired post-liquefaction shear strain per cycle. This parameter was calibrated simultaneously with calibrating the model to liquefy at 15 cycles with a goal to produce approximately 1.5%, 1.0%, and 0.5% post-liquefaction shear strain per cycle for $(N_1)_{60}$ values of 5, 15, and 25 respectively.
d_b	This parameter accounts for fabric damage in the dilation equation. In the absence of reliable laboratory data that quantifies fabric damage, this parameter was calibrated in combination with other dilation parameters to result in the desired post-liquefaction accumulation of shear strain.
d_c	This parameter accounts for the effects of overburden stress on the dilation rate (i.e. K_σ effect).
NYS	Number of yield surfaces
S_0	Shear strength at zero mean effective pressure. For sands, a post-liquefaction strength of 2 kPa was assumed which results in octahedral shear strength equal to 1.73 kPa based on $\eta_{2,p'=0} = \frac{2\sqrt{3}}{3}S_0$

effects of static shear stress on liquefaction triggering (resulting in a $K\alpha$ close to unity). The model was updated by introducing the second term to the flow rule in Eq. 7b (controlled by input parameter c_e). The CSR_0 term in this equation represents the static shear stress ratio. Comparisons of the $K\alpha$ parameter obtained from the updated model and experimental results are provided later. Since the additional terms presented in Eq. 7b are a function of CSR and CSR_0 , the model works well for problems where liquefaction is induced by seismically-induced shear wave propagation (resulting mainly in cyclic simple shear-type loading). It also captures the effects of the initial static shear stress (i.e. $K\alpha$) for situations of sloping ground.

2.4.2. Dilative phase

The dilative phase was developed in the original model to primarily capture cyclic mobility and post-liquefaction accumulation of shear strain. The equation for dilation was updated in the new model to capture the effects of effective overburden stress as shown by parameter d_c in the equation below. Dilation occurs only due to shearing outside the PT surface ($\eta > \eta_{PT}$ and $\dot{\eta} > 0$). The dilation flow rule is defined as:

$$P'' = \left(1 - \text{sign}(\dot{\eta}) \frac{\eta}{\eta_{PT}}\right)^2 (d_a + \gamma_d^{d_b}) \left(\frac{P_{atm}}{p'}\right)^{d_c} \quad (8)$$

where, d_a , d_b , and d_c are the model input parameters. Variable γ_d is an octahedral shear strain accumulated from the beginning of a particular dilation cycle as long as no significant load reversal happens. As a result, dilation rate increases as the shear strain in a particular cycle increases. A significant unloading that leads to dilation in the opposite direction will reset γ_d to zero.

The effects of input parameter d_a can be better observed on the shear stress-strain space in Fig. 6. Decreasing d_a reduces the dilative tendency and that, in return, increases the accumulated shear strain per cycle. Therefore, input parameter d_a can be used to adjust the accumulated shear strain per cycle to the desired range.

The effects of input parameter d_b are shown in Fig. 7. The term $\gamma_d^{d_b}$ in Eq. (8) accounts for the fabric damage. To assess the effects of this factor on strain accumulation it should be noted that γ_d is the octahedral shear strain accumulated in a single dilative cycle and it usually takes a value smaller than 1 in common engineering applications. Therefore, changing d_b from 3.0 to 0.3 increases the term $\gamma_d^{d_b}$ and results in a stronger dilative tendency which, in return, results in a smaller shear

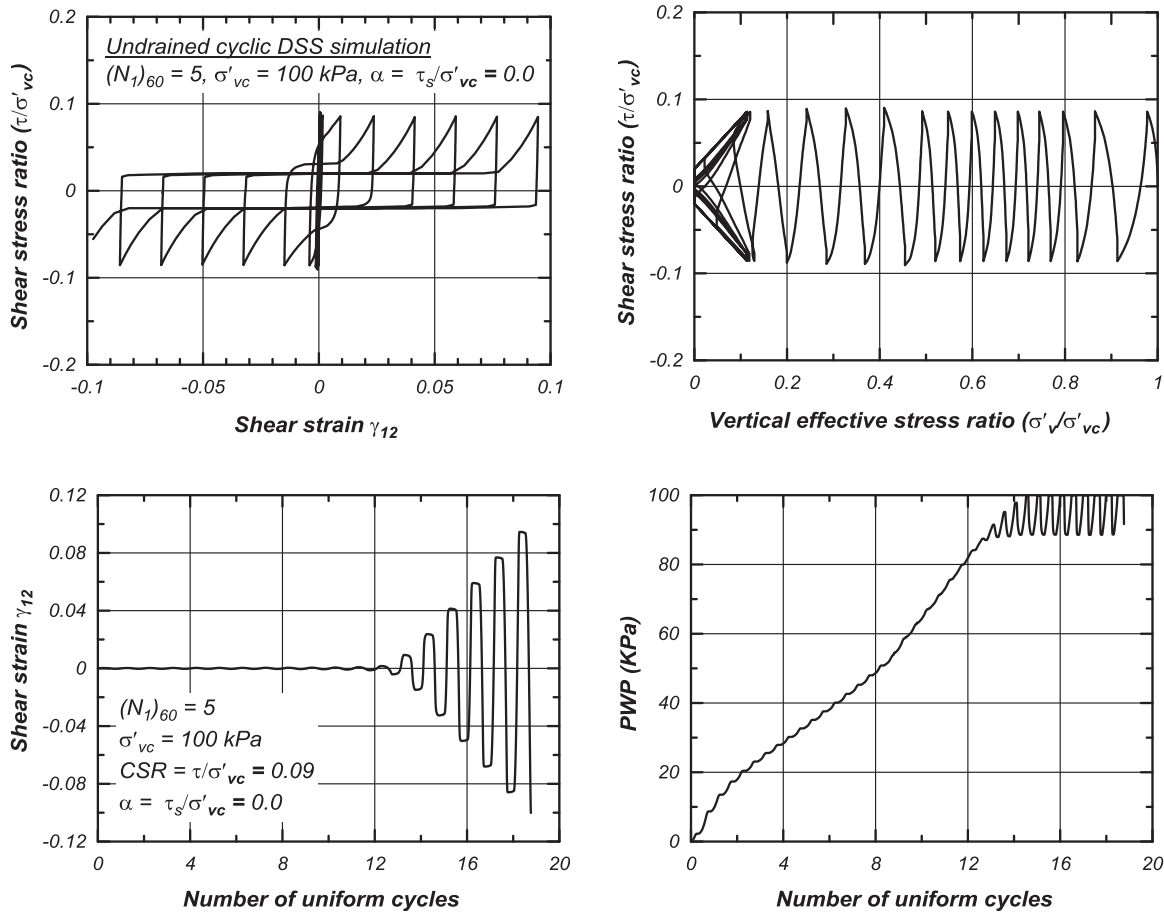


Fig. 9. Example model response in undrained cyclic simple shear loading for $(N_1)_{60} = 5$.

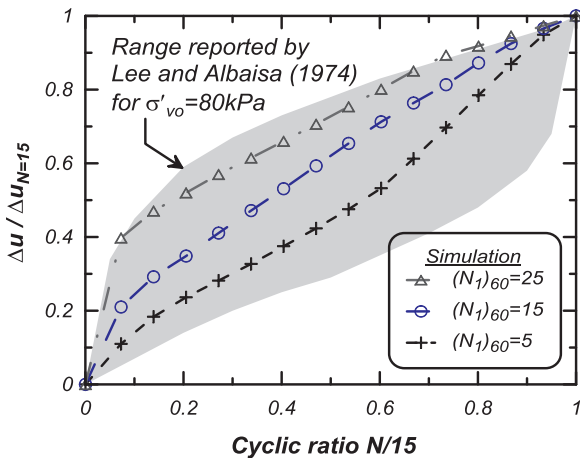


Fig. 10. Model predicted rate of pore pressure generation in DSS simulations for different relative densities at $\sigma'_{vc} = 100 \text{ kPa}$ compared with the range expected from experimental observations.

strain accumulation per cycle. The recommended value for d_b is 3.0 but the user can change it for a soil-specific calibration.

2.4.3. Neutral phase

When the stress state approaches the PT surface ($\eta = \eta_{PT}$) from below, a significant amount of permanent shear strain may accumulate prior to dilation, with minimal changes in the shear stress and p' , implying that $p'' \approx 0$. For simplicity, this phase is modeled by maintaining $p'' = 0$ during this highly yielding phase, until a boundary defined in

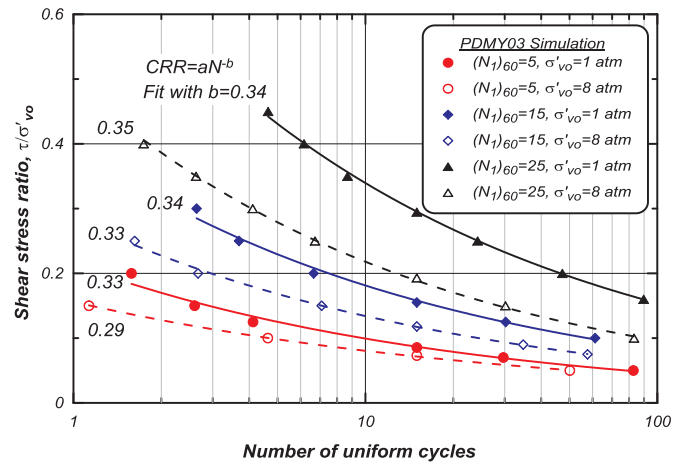


Fig. 11. Cyclic shear stress ratio versus number of uniform loading cycles in undrained DSS simulations to trigger liquefaction defined as single-amplitude shear strain of 3% (no static shear stress $\alpha = 0$).

the deviatoric strain space is reached, with subsequent dilation thereafter. This concept is shown in Fig. 8 and is denoted by phases 4–5 and 7–8. This domain will enlarge or translate depending on load history. The transformation of yield domain is explained in detail in Yang et al. [32].

3. Model calibration to engineering parameters

The primary focus in the calibration process was to capture

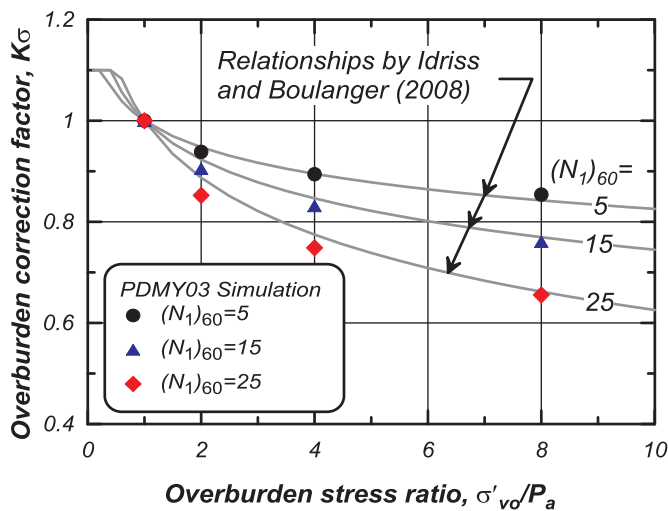


Fig. 12. K_σ relationships derived from model simulations compared to relationships by Idriss and Boulanger [14].

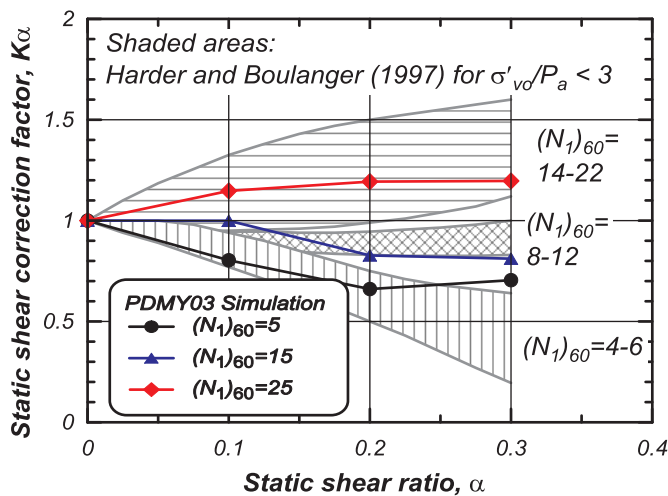


Fig. 13. Experimental trends for different $(N_1)_{60}$ values and $\sigma'_{vc} < 3$ atm from Harder and Boulanger [12] and model generated static shear stress correction factors (K_α) for $\sigma'_{vc} = 1$ atm.

earthquake-induced liquefaction triggering and post-liquefaction cyclic mobility based on empirical or mechanics-based correlations suggested by other researchers for siliceous clean sands. For a specific type of sand (e.g., calcareous sand) the model parameters should be calibrated to simulate the desired response based on experimental results. In light of relative complexity of the model and input parameters, the calibration is developed such that the user can extract the input parameters based solely on relative density (D_R) or SPT $(N_1)_{60}$ values for clean sand. For sands with significant fines content, the SPT $(N_1)_{60}$ values can be modified using correlations proposed by others (for example [14]).

The updated model was calibrated for plane-strain cyclic-undrained conditions. The analyses were performed in the OpenSees FE platform using the PDMY03 model. Table 1 provides the proposed calibrated input parameters for PDMY03 for four different relative densities. Table 2 provides a brief description for each parameter and the adopted calibration procedure.

4. Model responses

This section presents an element-level response of the model under undrained cyclic shear loading conditions. The simulations are performed for a range of different relative densities, cyclic stress ratios,

effective overburden stresses, and static shear stresses. The results are used to show the model's response against design relationships that are typically used to characterize and evaluate the dependence of liquefaction triggering to various factors such as the number of loading cycles, overburden effective stress, and static shear stress.

4.1. Example model response in undrained cyclic loading

Example element-level responses of cyclic simple shear tests (DSS) in undrained conditions are presented in this section. The analyses were performed in OpenSees FE platform with 9–4-QuadUP elements. The responses are shown for the Gauss integration point in the middle of the element. As described earlier, the contraction flow rule of the model was updated to account for the effects of initial static shear stress. This was achieved by incorporating the initial shear stress ratio in the contraction flow rule equation (i.e. CSR_0 in Eq. 7b). In a DSS simulation, a non-zero initial shear stress can be induced due to a locked-in horizontal shear stress ($\tau_{xy,0}$) to represent a sloped ground. The element was first consolidated under a vertical stress and drained conditions with boundaries fixed horizontally. The Poisson's ratio was set to 0.33 resulting in lateral earth pressure of $K_0 = 0.5$ during the gravity application. Subsequently, the element was subjected to shear cyclic loading. To simulate undrained conditions, the permeability was set sufficiently low to avoid drainage during shear loading (i.e. $1e-8$ m/s). The automatically generated modulus reduction curves (G/G_{max}) were adopted in these analyses. Fig. 9 shows representative simulation results of an undrained cyclic shear loading on a sand with $(N_1)_{60} = 5$ under the effective confining stress of 1 atm and no static shear stress ($\alpha = 0$). The element is subjected to a cyclic shear stress ratio (CSR) of 0.09 which results in a single-amplitude shear strain of 3% after 15 cycles.

4.2. Rate of excess pore water pressure generation in undrained loading

Fig. 10 shows the normalized excess pore water pressures for different relative densities as a function of normalized number of loading cycles. Also shown in this figure is the range of experimental observations reported by Lee and Albaisa [19]. The model response is reasonably bounded by the experimental data.

4.3. Effects of number of loading cycles on liquefaction triggering

Fig. 11 shows the cyclic stress ratio (CSR) to trigger liquefaction versus the number of loading cycles in undrained cyclic shear simulations. The results are shown for sands with $(N_1)_{60}$ values of 5, 15 and 25 (corresponding to relative densities (D_R) of 33%, 57% and 74%) under confining effective stress of 1 and 8 atm. The CRR is defined here as the ratio of horizontal shear stress (τ_{12}) to effective vertical stress (σ'_{v0}). The criterion for triggering of liquefaction is defined in this study as the moment at which a single-amplitude shear strain of 3% is reached. The model was calibrated to trigger liquefaction in 15 loading cycles at the CRR values estimated from the correlations by Idriss and Boulanger [14] and a vertical effective stress of $\sigma'_{v0} = 1$ atm. Also shown in this figure are the simulation results for the effective vertical stress of $\sigma'_{v0} = 8$ atm. The reduction in CSR due to a higher effective overburden stress is known as the K_σ effect which is discussed in the next section. Each curve in Fig. 11 is fitted with a power function ($CSR = a \cdot N^b$). The power (b-value) is shown for each curve ranging from 0.29 to 0.35. Experimental data suggest that the typical values for the power (b-value) should be approximately 0.34 for undisturbed frozen sand samples [34]. The updated contraction equation results in a reasonable agreement between the b-values from simulations and experiments.

4.4. Effects of effective overburden stress on liquefaction triggering (k_σ)

The dependence of CRR to the effective overburden stress is characterized by K_σ which is defined as $K_\sigma = CRR_{\sigma'_{v0}}/CRR_{\sigma'_{v0}=1atm}$. Fig. 12

shows $K\sigma$ from simulation results for effective overburden stresses ranging from 1 to 8 atm for sands with $(N_1)_{60}$ values of 5, 15 and 25. The recommended values by Idriss and Boulanger [14] are also shown in this figure. As implied from this figure, the model response is in good agreement with the recommended values across a wide range of effective overburden stress.

4.5. Effects of static shear stress on liquefaction triggering ($K\alpha$)

The influence of the static shear stress on liquefaction resistance is typically accounted for by a correction factor called $K\alpha$ defined as $K\alpha = CRR_{\alpha}/CRR_{\alpha=0}$ [28]. The in-situ static shear stresses are usually induced from sloped grounds. The majority of experimental studies on the $K\alpha$ effects are performed using DSS tests with locked-in horizontal shear stresses (e.g. [12]). Some experiments are also performed using Triaxial tests with anisotropic conditions (e.g. [31]). The $K\alpha$ factors in this study were evaluated in the context of locked-in static shear stress in simple shear simulations to represent the response of sloped ground. Model simulations were performed for a range of static shear stress ratios (α) under vertical effective stress of $\sigma'_{vo} = 1$ atm and the $K\alpha$ factors were subsequently generated for a range of relative densities. In each simulation, the vertical confinement and static shear stress were first applied statically under drained conditions. Thereafter, the element was subjected to undrained cyclic loading with CSR adjusted such that it would reach 3% single-amplitude shear strain in 15 cycles.

The $K\alpha$ factors derived from simulations are shown in Fig. 13. Also shown in this figure are experimental results from Harder and Boulanger [12]. It is observed that, in general, an increase in the static shear stress ratios (α) results in a decrease in $K\alpha$ for loose sands and an increase for dense sands. In other words, as the ground slope increases, loose sands will become more contractive and dense sand will become less contractive (more dilative). The $K\alpha$ factor can be adjusted using the input parameter c_e . Experimental and numerical studies have shown that $K\alpha$ could be dependent to the effective overburden stress as well [5,36]. However, the current implementation of PDMY03 does not directly account for this dependency. Future updates are possible to be implemented once sufficient laboratory data is available on the dependency of $K\alpha$ to the effective overburden stress.

5. Conclusions

The pressure-dependent multi-yield surface constitutive model was originally developed to capture cyclic mobility and post-liquefaction accumulation of shear strains. This paper presents new updates to the constitutive model to capture the effects of various parameters on triggering of liquefaction including the effects of the number of loading cycles, the effective overburden stress ($K\sigma$ effects), and the initial static shear stress ($K\alpha$ effects). The model has been improved with new flow rules to better simulate contraction and dilation induced by shear strains in soils, thereby more accurate modeling of liquefaction in sandy soils. The model has been implemented in 2D and 3D numerical platforms in OpenSees finite-element, and FLAC and FLAC^{3D} finite-difference frameworks.

The updated model has been calibrated based on design relationships for a range of relative densities for sand. Despite many input parameters that characterize the complex response of the constitutive model, different sets of input parameters are provided for generic response based on simple data available to designers, i.e. relative density of sand. The model parameters are calibrated for typical siliceous Holocene sands with different relative densities and are provided for cases where site-specific experimental data is not available.

This paper describes the basics of the plasticity framework of the model and provides guidelines to calibrate the input parameters of the model to simulate undrained cyclic loading conditions. The model responses under high effective overburden stress ($K\sigma$) and static shear stress ($K\alpha$) are compared to expected average behavior published by

other researchers showing reasonable agreements. Further developments are needed as new data become available.

Acknowledgments

The presented modifications to more formally capture the liquefaction triggering mechanism were motivated by the vision and related pioneering PM4Sand work of Professors Boulanger and Ziotopoulou. While at UCSD, the Initiatives of Dr. Zhaohui Yang addressed this vision with a preliminary effort. Dr. James Gingery provided valuable feedback during the preparation of this manuscript. The authors would like to thank the valuable comments by the two anonymous reviewers. Partial funding was provided by the National Science Foundation (NSF award OISE-1445712).

References

- [1] Andrianopoulos KI, Papadimitriou AG, Bouckovalas GD. Bounding surface plasticity model for the seismic liquefaction analysis of geotechnical structures. *J Soil Dyn Earthq Eng* 2010;30(10):895–911.
- [2] Andrus RD, Stokoe KH. Liquefaction resistance of soils from shear-wave velocity. *J Geotech Geoenviron Eng ASCE* 2000;126(11):1015–25.
- [3] Beaty MH. Application of UBCSAND to the LEAP centrifuge experiments. *J Soil Dyn Earthq Eng* 2018;104:143–53.
- [4] Boulanger RW. High overburden stress effects in liquefaction analysis. *J Geotech Geoenviron Eng ASCE* 2003;129(12):1071–82.
- [5] Boulanger RW. Relating $K\alpha$ to relative state parameter index. *J Geotech Geoenviron Eng ASCE* 2003;129(8):770–3.
- [6] Byrne PM, McIntyre J. Deformations in granular soils due to cyclic loading, Proceedings of Settlement 94, Texas. ASCE Geotechnical Special Publication No. 40; 1994. p. 1864–1896.
- [7] Chan AHC. A unified finite element solution to static and dynamic problems in geomechanics, Ph.D. Dissertation. Swansea, U.K.: Univ. College of Swansea.; 1988.
- [8] Cubrinovski M, Ishihara K. Modeling of sand behavior based on state concept. *Soils Found* 1998;38(3):115–27.
- [9] Dafalias YF, Manzari MT. Simple plasticity sand model accounting for fabric change effects. *J Geotech Geoenviron Eng ASCE* 2004;130(6):622–34.
- [10] Elgamal A, Yang Z, Parra E, Ragheb A. Modeling of cyclic mobility in saturated cohesionless soils. *Int J Plast* 2003;19(6):883–905.
- [11] Gingery JR, Elgamal A. Shear stress-strain curves based on the G/Gmax logic: A procedure for strength compatibility. In IACGE 2013: Challenges and Recent Advances in Geotechnical and Seismic Research and Practices; 2013. p. 721–729.
- [12] Harder LF, Boulanger RW. Application of $K\sigma$ and $K\alpha$ correction factors. Proceedings of the NCEER workshop on evaluation of liquefaction resistance of soils. Technical Report NCEER-97-0022, National Center for Earthquake Engineering Research, SUNY; 1997. p. 167–190.
- [13] Hill R. The mathematical theory of [lasticity. London: Oxford Univ. Press; 1950.
- [14] Idriss IM, Boulanger RW. Soil liquefaction during earthquakes. Monograph MNO-12. Oakland, CA: Earthquake Engineering Research Institute; 2008. [261p].
- [15] Itasca. FLAC – Fast lagrangian analysis of continua, version 7.0. Minneapolis, Minnesota: Itasca Consulting Group, Inc; 2011.
- [16] Itasca. FLAC3D – Fast lagrangian analysis of continua in 3 dimensions, Version 5.0. Minneapolis, Minnesota: Itasca Consulting Group, Inc.; 2013.
- [17] Iwan WD. On a class of models for the yielding behavior of continuous and composite systems. *J Appl Mech ASME* 1967;34:612–7.
- [18] Kramer SL. Geotechnical earthquake engineering. NJ: Prentice Hall; 1996.
- [19] Lee KL, Albaisa A. Earthquake induced settlements in saturated sands: 9F, 2T, 29R. *J. Geotech. Eng. DIV. V100, N. GT4, APR. 1974, P387–406. International Journal of Rock Mechanics and Mining Sciences & Geomechanics Abstracts, 11, 8. Pergamon; 1974.*
- [20] Li XS, Dafalias YF. Dilatancy for cohesionless soils. *Geotechnique* 2000;50(4):449–60.
- [21] Manzari MT, Dafalias YF. A critical state two-surface plasticity model for sands. *Geotechnique* 1997;49(2):252–72.
- [22] Marti J, Cundall P. Mixed discretization procedure for accurate modelling of plastic collapse. *Int J Numer Anal Methods Geomech* 1982;6:129–39.
- [23] Mazzoni S, McKenna F, Scott MH, Fenves GL. Open system for earthquake engineering simulation user manual. Berkeley: University of California; 2009.
- [24] Mroz Z. On the description of anisotropic work hardening. *J Mech Phys Solids* 1967;15:163–75.
- [25] Papadimitriou AG, Bouckovalas GD, Dafalias YF. Plasticity model for sand under small and large cyclic strains. *J Geotech Geoenviron Eng ASCE* 2001;127(11):973–83.
- [26] Parra E. Numerical modeling of liquefaction and lateral ground deformation including cyclic mobility and dilation response in soil systems [Ph.D. Thesis]. Troy, NY: Dept. of Civil Engineering, RPI; 1996.
- [27] Prevost JH. A simple plasticity theory for frictional cohesionless soils. *Soil Dyn Earthq Eng* 1985;4(1):9–17.
- [28] Seed HB, Idriss IM. Ground motions and soil liquefaction during earthquakes 5. Earthquake Engineering Research Institute; 1982.

- [29] Silver ML, Chan CK, Ladd RS, Lee KL, Tiedemann DA, Townsend FC, Valera JE, Wilson JH. Cyclic triaxial strength of standard test sand. *Journal of Geotechnical and Geoenvironmental Engineering*, 102 (ASCE# 12145 Proceeding); 1976.
- [30] Toki S, Tatsuoka F, Miura S, Yoshimi Y, Yasuda S, Makihara Y. Cyclic undrained triaxial strength of sand by a cooperative test program. *Soils Found* 1986;26(3):117–28.
- [31] Vaid YP, Chern JC. Cyclic and monotonic undrained response of saturated sands. *Adv Art Test Soils Cycl Cond* 1985:120–47.
- [32] Yang Z, Elgamal A, Parra E. Computational model for cyclic mobility and associated shear deformation. *J Geotech Geoenviron Eng* 2003;129(12):1119–27.
- [33] Yang Z, Elgamal A. Numerical Modeling of Earthquake Site Response Including Dilation and Liquefaction. Report No. SSRP-2000/01, Department of Structural Engineering, University of California, San Diego; 2000.
- [34] Yoshimi Y, Tokimatsu K, Kaneko O, Makihara Y. Undrained cyclic shear strength of dense Niigata sand. *Soils Found, Jpn Soc Soil Mech Found Eng* 1984;24(4):131–45.
- [35] Ziotopoulou K, Boulanger RW. Calibration and implementation of a sand plasticity plane-strain model for earthquake engineering applications. *J Soil Dyn Earthq Eng* 2013;53:268–80.
- [36] Ziotopoulou K, Boulanger RW. Plasticity modeling of liquefaction effects under sloping ground and irregular cyclic loading conditions. *Soil Dyn Earthq Eng* 2016;84(2016):269–83.